Energy Conversion and Management 156 (2018) 301–316

Contents lists available at ScienceDirect

Energy Conversion and Management

journal homepage: www.elsevier.com/locate/enconman

Towards accurate CFD simulations of vertical axis wind turbines at different tip speed ratios and solidities: Guidelines for azimuthal increment, domain size and convergence

Abdolrahim Rezaeiha[a,*], Hamid Montazeri[a,b], Bert Blocken[a,b]

[a] Building Physics and Services, Department of the Built Environment, Eindhoven University of Technology, P.O. Box 513, 5600 MB Eindhoven, The Netherlands;
[b] Building Physics Section, Department of Civil Engineering, KU Leuven, Kasteelpark Arenberg 40 – Bus 2447, 3001 Leuven, Belgium

ARTICLE INFO

Keywords:
Wind energy
Vertical axis wind turbine (VAWT)
CFD
URANS
Guideline
Aerodynamic performance

ABSTRACT

The accuracy of CFD simulations of vertical axis wind turbines (VAWTs) is known to be significantly associated with the computational parameters, such as azimuthal increment, domain size and number of turbine revolutions before reaching a statistically steady state condition (convergence). A detailed review of the literature, however, indicates that there is a lack of extensive parametric studies investigating the impact of the computational parameters. The current study, therefore, intends to systematically investigate the impact of these parameters, on the simulation results to guide the execution of accurate CFD simulations of VAWTs at different tip speed ratios (λ) and solidities (σ). The evaluation is based on 110 CFD simulations validated with wind-tunnel measurements for two VAWTs. Instantaneous moment coefficient, C_m, and power coefficient, C_P, are studied for each case using unsteady Reynolds-averaged Navier-Stokes (URANS) simulations with the 4-equation transition SST turbulence model. The results show that the azimuthal increment dθ is largely dependent on tip speed ratio. For moderate to high λ, the minimum requirement for dθ is 0.5° while this decreases to 0.1° at low to moderate λ. The need for finer time steps is associated to the flow complexities related to dynamic stall on turbine blades and blade-wake interactions at low λ. In addition, the minimum distance from the turbine center to the domain inlet and outlet is 15 and 10 times the turbine diameter, respectively. It is also shown that 20–30 turbine revolutions are required to ensure statistically converged solutions. The current findings can serve as guidelines towards accurate and reliable CFD simulations of VAWTs at different tip speed ratios and solidities.

1. Introduction

Vertical-axis wind turbines (VAWTs) have recently received great interest for wind energy harvesting both for off-shore applications [1,2] and in the built environment [3–5]. VAWTs have several advantages compared to horizontal-axis wind turbines (HAWTs) such as omni-directional capability, low manufacturing/installation/maintenance costs, robustness, scalability and low noise [6,7]. A detailed evaluation of the aerodynamic performance of VAWTs is a difficult task as the flow in such systems is complicated by phenomena such as dynamic stall [8,9], blade-wake interactions [10] and flow curvature effects [11,12]. Different experimental and numerical approaches have been employed to investigate this complex flow to evaluate the aerodynamic performance of VAWTs. Computational Fluid Dynamics (CFD) is a very useful tool for such evaluations, and has thus been widely used to investigate the aerodynamic performance of VAWTs [6,13–21]. Previous CFD studies included efforts to clarify the underlying physics behind the unsteady power conversion of the turbine [22–27] and to characterize the aerodynamic performance of VAWTs under the influence of various geometrical [28–34] and operational [35–38] parameters. In addition, several CFD studies focused on improving the aerodynamic performance of VAWTs by optimizing the pitch angle [39], minimizing the turbine power loss due to the presence of the shaft [40], employment of guide vanes, ducts [41–43] and flow control devices [44–46].

It is widely recognized that the accuracy and reliability of CFD simulations of VAWTs can be very sensitive to the computational settings. For example, earlier studies have shown the significant importance of azimuthal increment [6,47–51] and domain size [6,50,52,53]. However, the results of these studies are case-specific and limited in scope where the conclusions did not (aim to) provide generally valid recommendations and guidelines to support future CFD studies of VAWTs. Therefore, there is no consensus on the employed computational settings for the Unsteady Reynolds-averaged Navier-Stokes (URANS) simulations of VAWTs in the literature. This is

* Corresponding author.
E-mail address: a.rezaeiha@tue.nl (A. Rezaeiha).

https://doi.org/10.1016/j.enconman.2017.11.026
Received 20 September 2017; Received in revised form 26 October 2017; Accepted 11 November 2017
Available online 01 December 2017

Nomenclature

A	swept area, $H{\cdot}D$ [m^2]
BR	blockage ratio (D/W) [–]
c	blade chord length [m]
C_m	instantaneous moment coefficient [–]
C_P	power coefficient, $P/(qAU_\infty)$ [–]
C_T	thrust coefficient, $T/(qA)$ [–]
D	turbine diameter [m]
d_c	diameter of rotating core [m]
d_i	distance from turbine center to domain inlet [m]
d_o	distance from turbine center to domain outlet [m]
dt	time step [s]
$d\theta$	azimuthal increment [°]
H	turbine height [m]
L	domain length [m]
L_w	length of the turbine wake [m]
M	moment [Nm]
n	number of blades [–]
P	turbine power [W]
q	dynamic pressure [Pa]
R	turbine radius [m]
Re_c	chord-based Reynolds number, $(c{\cdot}\sqrt{(R\Omega)^2 + U_\infty^2})/\nu$ [–]
Re_θ	momentum-thickness Reynolds number [–]
T	thrust force [N]
U	velocity magnitude [m/s]
U_∞	freestream velocity [m/s]
v	lateral velocity [m/s]
W	domain width [m]
γ	intermittency [–]
λ	tip speed ratio, $\Omega{\cdot}R/U_\infty$ [–]
ν	kinematic viscosity [m^2/s]
θ	azimuthal angle [°]
σ	solidity, $n{\cdot}c/D$ [–]
ω	specific dissipation rate [1/s]
Ω	rotational speed [rad/s]

especially the case for azimuthal increment, domain size and convergence criterion (defined as number of turbine revolutions before reaching a statistically steady state condition), as an extensive review of CFD studies of VAWTs indicates that:

- The range of the azimuthal increment (which is defined as the number of degrees that a turbine rotates per time step) varies from 0.03° [6,48] to 10° [6,54,55].
- The size of the computational domains varies from very small to very large values. For example, for the downstream length the variation is from less than 10D (D: turbine diameter) [54–57] to more than 50D [6,50]. For the upstream length the variation is from less than 5D [54–57] to more than 15D [6,50].
- There is no clear consensus on the convergence criterion. Some studies [56] considered convergence from the 4th turbine revolution while other studies considered this from 100th turbine revolution [6].

To the best of our knowledge, the first study to derive the minimum requirements for computational settings of CFD simulations was performed by Rezaeiha et al. [6]. The results of that study showed that:

- Employment of an azimuthal increment of 5° would lead to 17% underprediction of turbine C_P.
- Using a computational domain with 5D distance from the turbine center to domain inlet results in more than 5% overprediction of turbine C_P.
- Sampling data starting after the 5th turbine revolution would result in more than 20% overprediction of turbine C_P.

It should be noted that the study by Rezaeiha et al. [6] was only performed for a low solidity ($\sigma = 0.12$) and moderate tip speed ratio ($\lambda = 4.5$). Those parameters were selected to minimize the flow complexity associated to dynamic stall [8], blade-wake interactions [10] and flow curvature effects [12]. Nevertheless, the more complex flows for lower tip speed ratios might bring more challenges to CFD simulations, which might influence the minimum requirements for computational settings and parameters. To the best of our knowledge, there is a lack of sensitivity analysis for minimum requirements for computational settings and parameters for CFD simulations of VAWTs at different tip speed ratios and solidities. The current study, therefore, intends to systematically investigate the impact of azimuthal increment, domain size and convergence criterion on the simulation results at different tip speed ratios and solidities to guide the execution of accurate CFD simulations of VAWTs.

The outline of the paper is as follows: the geometrical and operational characteristics of the wind turbine and the computational settings are described in Section 2.1–2.3. A reference case for the sensitivity analysis is defined in Section 2.4. Solution verification and validation studies are presented in Section 3. The sensitivity of the minimum requirements for azimuthal increment, domain size (distance from the turbine center to the domain inlet and outlet) and convergence criterion to tip speed ratio and solidity is extensively discussed in Sections 4–7, respectively. The discussion and the conclusions are provided in Section 8–9.

2. Computational settings and parameters

2.1. Geometrical and operational characteristics of the reference case

An H-type vertical axis wind turbine with 2 blades of symmetric NACA0018 airfoil section is used. The turbine has a diameter (D) of 1 m and a shaft diameter of 0.04 m. The turbine and the shaft rotate counter- clockwise with the same rotational speed. The freestream velocity (U_∞) is 9.3 m/s with a total turbulence intensity of 5%. The same freestream velocity as in the validation study for the reference turbine (see Section 3) is used. The turbine chord-based Reynolds number (Re_c) is 176,000. The turbine for the reference case has a solidity (σ) of 0.12, a chord length (c) of 0.06 m and a turbine rotational speed (Ω) of 83.8 rad/s (800 rpm), leading to a tip speed ratio (λ) of 4.5. Tip speed ratio and solidity are defined using Eqs. (1) and (2). The main geometrical and operational characteristics of the turbine for the reference case are shown in Fig. 1 and described in Table 1. Note that these characteristics are the same as those used in the earlier study by Rezaeiha et al. [6] in which guidelines for the minimum domain size and azimuthal increment for a low-solidity ($\sigma = 0.12$) VAWT operating at a moderate tip speed ratio of 4.5 were provided.

$$\lambda = \frac{R\Omega}{U_\infty} \tag{1}$$

$$\sigma = \frac{nc}{D} \tag{2}$$

2.2. Computational domain and grid

Fig. 2 illustrates the two-dimensional (2D) computational domain employed in this study. Note that the use of a 2D domain is based on the results of the study by Rezaeiha et al. [6,38] in which a detailed

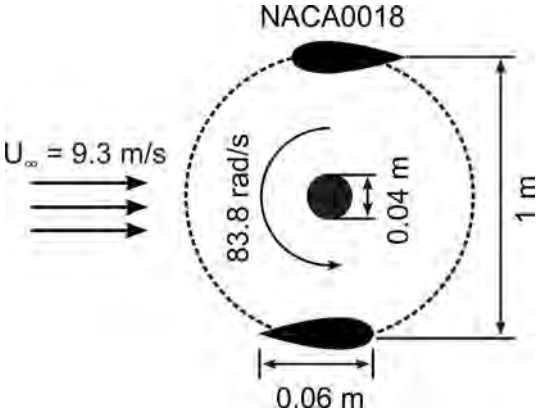

Fig. 1. Schematic of the turbine for the reference case (not to scale).

Table 1
Geometrical and operational characteristics of the VAWT for the reference case.

Parameter	Value	Parameter	Value
Number of blades, n	2	Blade aspect ratio, H/c	16.67
Diameter, D [m]	1	Shaft diameter [m]	0.04
Swept area, A [m2]	1	Tip speed ratio, λ [–]	4.5
Airfoil	NACA0018	Freestream velocity, U_∞ [m/s]	9.3
Airfoil chord, c [m]	0.06	Freestream total turbulence intensity	5%
Solidity, σ [–]	0.12	Rotational speed, Ω [rad/s]	83.8

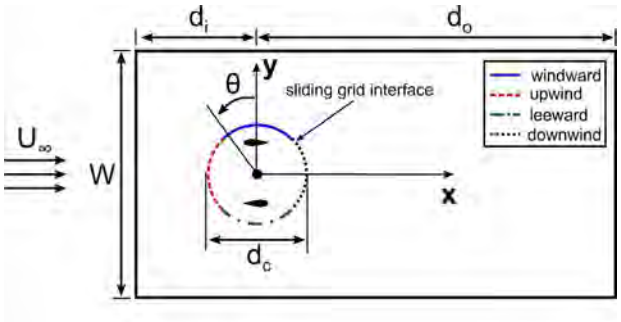

Fig. 2. Schematic of the computational domain: d_i and d_o, distance from the turbine center to the inlet and outlet; d_c, diameter of the rotating core; W, width of the domain.

sensitivity analysis was performed for 2D and 2.5D computational domains with the reference turbine and a systematic difference in the calculated C_P values were observed. The 2D domain represents the mid-plane of a high blade-aspect-ratio (H/c) turbine where the 3D tip effects are minimized [26]. In this study, the blade-aspect-ratio for the reference turbine is 16.67.

Earlier studies have shown that for CFD simulations of VAWTs, a blockage ratio of less than 5% (a minimum domain width of 20D) is required to minimize the effect of side boundaries on the results [6]. For 2D simulations, the blockage ratio is defined as D/W where D and W correspond to the turbine diameter and domain width. As the blockage ratio is defined based on the full diameter of the turbine, it is assumed to be not significantly affected by the turbine tip speed ratio and solidity. Therefore, in the present study, the domain width of 20D is employed. In addition, the impact of the diameter of the rotating core d_c (the rotating region of the domain which is connected to the fixed domain using a sliding grid interface as shown in Fig. 2) was found to be very negligible (< 0.04%) on the calculated turbine performance [6]. In the present study, therefore, the diameter of the rotating core is 1.5D. The rotating core is joined to the surrounding fixed domain using a sliding grid interface. The distance from the turbine center to domain inlet (d_i) and outlet (d_o) for the reference case are 5D, 25D, respectively. Four quartiles are defined on the plane of rotation of the blades [58], namely windward $315° \le \theta < 45°$, upwind $45° \le \theta < 135°$, leeward $135° \le \theta < 225°$ and downwind $225° \le \theta < 315°$. Azimuthal angle θ is defined based on the position of the top blade (which is currently positioned the most windward) as shown in Fig. 2.

The computational grid is made up of quadrilateral cells everywhere. The maximum cell skewness in the grid is 0.55 and the minimum orthogonal quality is 0.21. The maximum y^+ values on the surfaces of the blades and the shaft are 4 and 2, while the average y^+ values are 1.37 and 1.02, respectively. The total number of cells is approximately 400,000. Fig. 3 shows the computational grid. The boundary conditions are uniform velocity inlet, zero gauge pressure outlet, symmetry sides and no-slip walls. The turbulent length scale at the domain inlet and outlet is selected based on the length scale of the interest, i.e. turbine diameter, 1 m.

2.3. Other numerical settings

Incompressible unsteady Reynolds-averaged Navier-Stokes (URANS) simulations are performed using the commercial CFD software package ANSYS Fluent 16.1. The computational settings are based on an earlier solution verification and validation study [6]. Second-order schemes are used for both temporal and spatial discretization. The SIMPLE scheme is used for pressure-velocity coupling.

Turbulence is modeled using the 4-equation transition SST turbulence model, also known as γ-θ SST turbulence model [59], which is an improvement over the two-equation k-ω SST turbulence model [60,61]. The model solves two additional equations for intermittency γ and momentum-thickness Reynolds number Re_θ to provide a more accurate prediction of laminar-to-turbulent transition for wall-bounded flows where such prediction is critical to correctly model the boundary layer development and to calculate the loads on the walls [62,63]. Further details of the γ-θ SST turbulence model are provided by Menter et al.

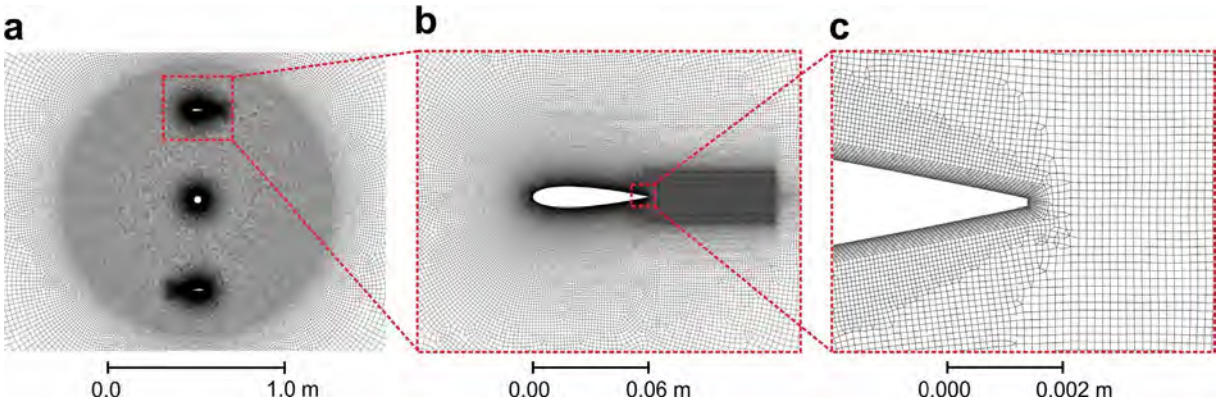

Fig. 3. Computational grid: (a) near the rotating core; (b) near the airfoil; (c) near the airfoil trailing edge.

Table 2
The computational settings for the reference case.

d_i	d_o	W	d_c	Domain size (L × W)	dθ	# turbine revolutions
5D	25D	20D	1.5D	30D × 20D	0.1°	20

[59] and Langtry et al. [63]. Modeling of the laminar-to-turbulent transition using intermittency-based models has also been proven successful by Suzen et al. [64,65], Walters and Leylek [66], Cutrone et al. [67] and Genç et al. [68–73] for flow on airfoils, which further provides confidence for application of these models. Note that the ω-based turbulence models benefit from a y^+-insensitive formulation which means that the model, based on the y^+ of the cells near the wall, will either opt for the low-Reynolds modeling, to resolve the buffer layer and viscous sublayer near the wall, or for wall functions [61,74,75].

The unsteady simulations are initialized with the solutions of steady RANS simulations and continued for 20 turbine revolutions. The azimuthal increment (dθ) employed for the unsteady calculations for the reference case is 0.1°. Each time step consists of 20 iterations to have the scaled residuals $< 1 \times 10^{-5}$. The instantaneous moment coefficient is sampled at the 21st turbine revolution and the values are employed to calculate the turbine power coefficient.

2.4. Reference case

The computational settings for the reference case is described in Table 2. The sensitivity analysis is performed for domain size, azimuthal increment and convergence criterion (defined as number of turbine revolutions before reaching a statistically steady state condition) by applying systematic changes to the reference case. In Sections 4–7, one of the computational settings is varied, while all others are kept the same as in the reference case. In the current study, tip speed ratio is modified by altering the turbine rotational speed and solidity is modified by altering the blade chord length.

Because the flow velocity coming to the blade, the experienced velocity, is the vector sum of the freestream velocity and the rotational velocity, therefore, modifying the experienced velocity via changing either of the two is expected to have similar results on the derived minimum requirements. In the present study, the experienced velocity is modified by changing the rotational velocity. Note that changing the experienced velocity will change Re_c and can also alter λ. While the impact of λ on the derived minimum requirements is investigated in the present study, the investigation of the dependence of the derived minimum requirements on Re_c is proposed for future research.

3. Solution verification and validation

Solution verification and two sets of validation studies are performed. Because these studies have been published as separate papers [6,39], only the headlines are briefly repeated here. The verification studies were performed for the reference case, described in Section 2.4. The following observations were made [6]:

- A grid sensitivity analysis was performed using three grids which were uniformly refined by √2. Grid Convergence Index (GCI) [76] was calculated based on C_P values using a safety factor F_s of 1.25. For the coarse-medium grid pair, GCI^{coarse} and GCI^{fine} was 6.1×10^{-3} and 3.5×10^{-3}, which represent 1.48% and 0.85% of the respective C_P values.
- A time step sensitivity analysis was performed where an azimuthal increment of 0.5° was found to be sufficient. Further refinement of the time step to 0.1° had negligible (< 1%) effects on C_P values.
- An iterative convergence study was performed where a statistically steady state solution was obtained after 20–30 turbine revolutions. The difference between C_P values at 20 and 30 revolutions with that of 100 revolutions was found to be 2.41 and 1.06%, respectively.
- A comparative study was performed where the results of the 2D domain were compared with that of a 2.5D with span of 6 cm (1 blade chord length). The comparison showed a systematic difference of approximately 6% in the C_P values [38].

The first validation study [6], which was performed for the reference case, compared the CFD results against the experimental data by Tescione et al. [26]. The comparison of the time-averaged normalized streamwise and lateral velocities in the near wake of the turbine at different downstream locations from x/R = 2.0–3.0 showed a deviation of 8.6–11.8% for the streamwise component and 2.3–2.5% for the lateral component, respectively.

The second validation study [39], which was performed for a 3-bladed VAWT, compared the CFD results against the experimental measurements by Castelli et al. [77]. The comparison of turbine C_P for 8 different tip speed ratios $1.44 \le \lambda \le 3.29$, shown in Fig. 4a, confirmed that the CFD results were in line with the experimental data. In addition, the figure shows that substantial improvement was achieved compared to the numerical results by Castelli et al. [77]. The good agreement observed for different tip speed ratios shows that the simulations could provide a reasonable prediction of the turbine performance also for lower λ (≤2.33) where the occurrence of dynamic stall results in a complex flow over the turbine blades. The occurrence of

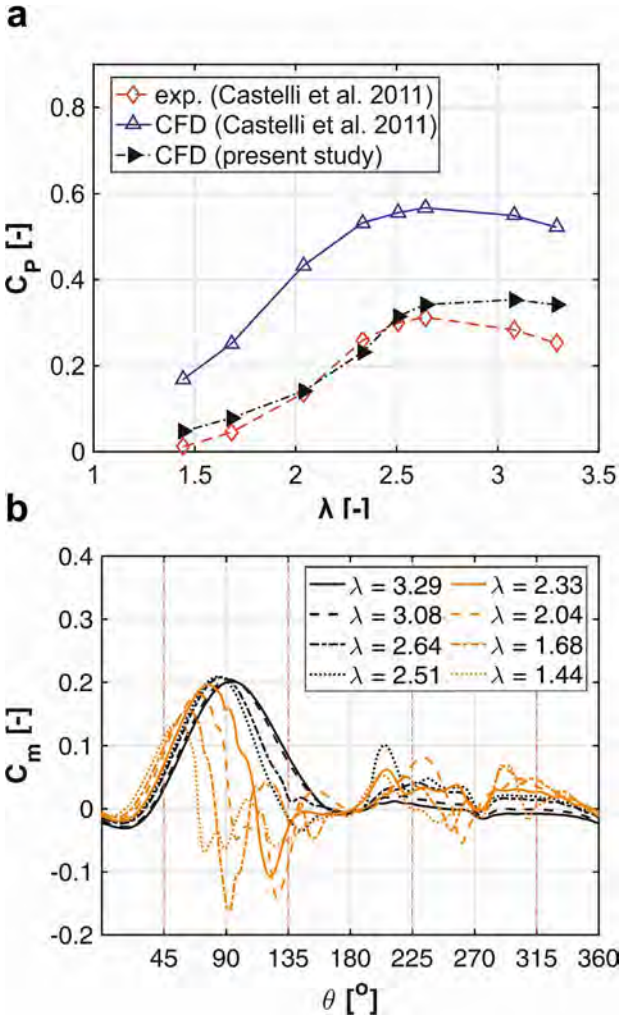

Fig. 4. (a) Comparison of power coefficient from the present study against experiment [77,78] and other 2D CFD results [77]; (b) instantaneous moment coefficient during the last turbine revolution for different tip speed ratios.

Table 3
Description of cases for the study of azimuthal increment dθ.

d_i/D	d_o/D	Domain size (L/D) × (W/D)	dθ [°]	λ	σ
5†	25†	30 × 20†	0.025, 0.05, 0.1†, 0.5, 1.0	1.5, 2.5, 3.0, 3.5, 4.5†, 5.5	0.06, 0.09, 0.12†, 0.18, 0.24

Note: The reference case is shown with '†' sign.

dynamic stall for $\lambda \leq 2.33$ is confirmed from the instantaneous moment coefficient on the blades as shown in Fig. 4b. The possible explanations for the observed deviation between the present CFD results and the experimental data are extensively discussed in Refs. [6,39].

4. Azimuthal increment

The minimum required time step of the URANS simulations is driven by the time scales of the unsteady complex phenomena occurring in the flow. For the case of wind turbines, it is customary to correlate the time step with the turbine revolution and express it as azimuthal increment dθ. Azimuthal increment is then defined as the number of degrees that the turbine rotates per time step. As the complexity of the flow on VAWTs varies with the operating conditions and geometrical parameters, i.e. λ and σ, therefore, a sensitivity analysis is performed for dθ by applying systematic changes to the reference case. In this section, the sensitivity of the minimum requirements for the dθ to different tip speed ratios and solidities are investigated where the details of the computational parameters for all the cases are presented in Table 3.

4.1. Dependency on tip speed ratio

Fig. 5 indicates the instantaneous moment coefficient C_m for the last turbine revolution versus azimuth θ for tip speed ratios $1.5 \leq \lambda \leq 5.5$ calculated using different azimuthal increments $0.05^\circ \leq d\theta \leq 1.0^\circ$. The turbine solidity is 0.12, which is the same as the reference case. It can be seen that for relatively high tip speed ratios of 4.5 and 5.5 the difference between the results for $d\theta \leq 0.5^\circ$ is negligible (Fig. 5a-b). The main reason is that moderate to high tip speed ratios of 4.5 and 5.5 correspond to a regime where the flow is mostly attached and the variations of the angle of attack on the blades during the turbine

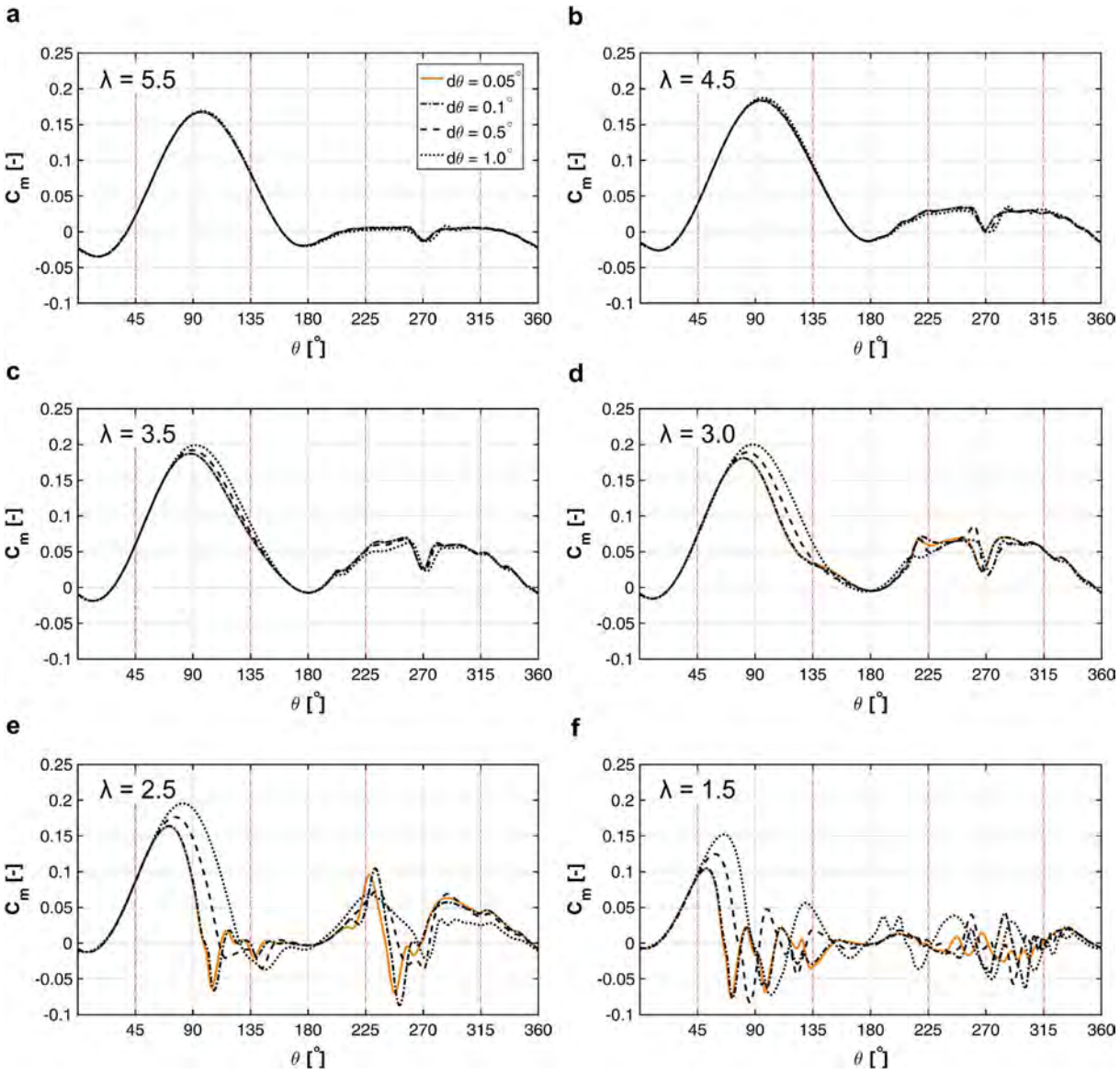

Fig. 5. Instantaneous moment coefficient for the last turbine revolution for different tip speed ratios using various azimuthal increments. (σ = 0.12).

revolution are limited below the static stall angle. Consequently, the flow physics are less complex compared to those at lower λ values due to the absence of dynamic stall and blades' wake-blade interactions. A closer look at Fig. 5a and b indicates small deviations for dθ = 1.0° on the downwind side around θ = 270°, corresponding to the wake of the shaft [40]. This confirms that even at relatively high λ values, the interactions between the vortices shed from the shaft and the blades passing in the shaft wake (shaft's wake-blade interaction) can make predictions of the flow more challenging. In this case, finer azimuthal increments are required.

For low to moderate tip speed ratios λ < 4.5 (Fig. 5c–f), where the variations of the angle of attack on the blades get larger and consequently dynamic stall and blade-wake interactions would occur, the results are highly dependent on azimuthal increments. The difference is mainly observed in two regions: upwind (45° < θ < 135°) and downwind (225° < θ < 315°). The former is associated with the occurrence of the dynamic stall, which happens at such azimuthal angles and results in a sudden drop in C_m. The latter corresponds to the interactions of the vortices shed from the blades in the upwind and the shaft with the blades passing downwind (blade-wake interactions) and results in strong fluctuations in C_m [40,79,80]. The accurate predication of the flow complexities associated with the two phenomena, therefore, requires a fine azimuthal increment. The lines corresponding to dθ = 0.1° and 0.05° almost overlap for all the cases implying that the solution is no longer dependent on dθ.

Fig. 6a shows how dθ affects the turbine power coefficient for different values of λ. For λ ≥ 4.5, it can be seen that dθ has limited effects on the turbine C_P, though it can lead to a better prediction of the shaft's wake-blade interaction, as shown in C_m curves in Fig. 5a and b.

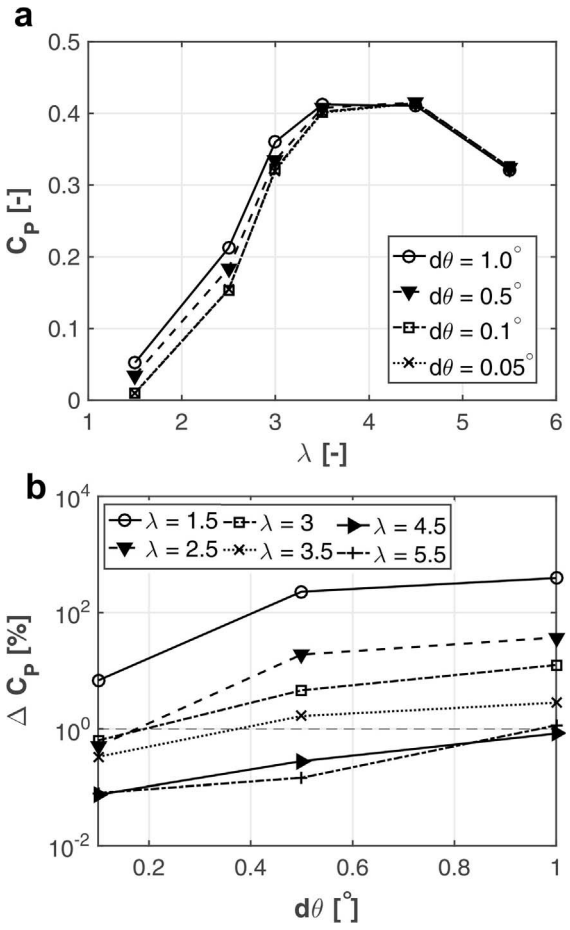

Fig. 6. (a) Power coefficient and (b) its relative change with respect to $d\theta = 0.05°$ for different tip speed ratios calculated using various azimuthal increments. (σ = 0.12).

The increased deviation between the results of simulations using fine (0.05°–0.1°) and coarse (0.5°–1.0°) dθ with reducing λ (< 4.5) is also apparent from the predicted turbine C_P shown in Fig. 6a. The results start to deviate at λ = 3.5. The deviation in terms of C_P increases as λ reduces to 2.5 and then stays almost constant when λ further reduces to 1.5. This suggests that at 2.5 < λ ≤ 3.5, the separation is still growing on the blades by reducing λ, and there is a light stall. For 1.5 ≤ λ ≤ 2.5, the blades have already gone through a deep stall, and further reduction in λ from 2.5 to 1.5 might not bring more complexities in the flow. This is in line with the trend observed for C_m in Fig. 5c-f where the typical signatures of the dynamic stall (sudden drop in loads and follow-up fluctuations) are pronounced for 1.5 ≤ λ ≤ 2.5 (Fig. 5e–f) but not present for 2.5 < λ ≤ 3.5 (Fig. 5c and d). The figure also confirms that the predicted turbine C_P using dθ of 0.1° and 0.05° are the same for all λ values from 1.5 to 5.5. It can be concluded that for the solidity of 0.12, dθ = 0.1° is sufficient to capture the complex phenomena of dynamic stall on the turbine blades and further refinement in time step would not have any significant effects on the results.

Fig. 6b shows the difference between the calculated C_P obtained using different values of dθ and that obtained using the finest dθ. For λ > 3.5, it can be seen that for dθ = 0.5°, ΔC_P is less than 1%. Therefore, an azimuthal increment of 0.5° is found to be the minimum requirement for moderate to high λ (> 3.5). The figure shows that ΔC_P drops below 1% using dθ = 0.1° for all λ values, except for λ = 1.5, which is associated with the very low C_P values at such λ. For λ = 1.5, this is further confirmed by the fact that ΔC_P calculated using dθ of 0.05° and 0.025° does not show any further reduction. Based on the above discussions, the minimum requirements for azimuthal increment as a function of tip speed ratio is presented in Table 4. Two operating regimes are considered: (i) low to moderate λ and (ii) moderate to high λ. For the given turbine with a solidity of 0.12, the former regime corresponds to 1.5 ≤ λ ≤ 3.5 while the latter corresponds to 3.5 < λ ≤ 5.5. For low to moderate λ, the minimum requirement is dθ = 0.1° while for moderate to high λ this value can go up to dθ = 0.5°.

4.2. Dependency on solidity

Fig. 7 shows the instantaneous moment coefficient C_m for the last turbine revolution versus azimuth θ for different solidities 0.06 ≤ σ ≤ 0.24 and azimuthal increments 0.05° ≤ dθ ≤ 0.5°. Fig. 8 shows the predicted C_P for different solidities calculated using different values of dθ. The tip speed ratio is 4.5, which is the same as the reference case. To reduce the computational cost, the azimuthal increment of 1.0° is no longer considered as the minimum requirement derived in Section 4.1 is 0.5° and dθ = 1.0° is thus considered to be too coarse. It can be seen that for 0.09 ≤ σ ≤ 0.24 (Fig. 7a–d), no significant difference is observed for different values of azimuthal increments. The C_m values in the downwind near θ ≈ 270° show that as solidity decreases (airfoil chord-length decreases), the effect of the shaft's wake interaction with blades passing downstream becomes more pronounced. This is due to the increase in the relative length scale of vortices shed from the shaft to the airfoil chord. The more blade-wake interactions result in very small deviations in C_m in the shaft wake

Table 4
The minimum requirement for azimuthal increment as a function of tip speed ratio. (σ = 0.12 for all cases).

λ	Value	dθ [°]	Re_c (×10^3)
Moderate to high	5.5	0.5	214
	4.5	0.5	176
Low to moderate	3.5	0.1	139
	3	0.1	121
	2.5	0.1	103
	1.5	0.1	69

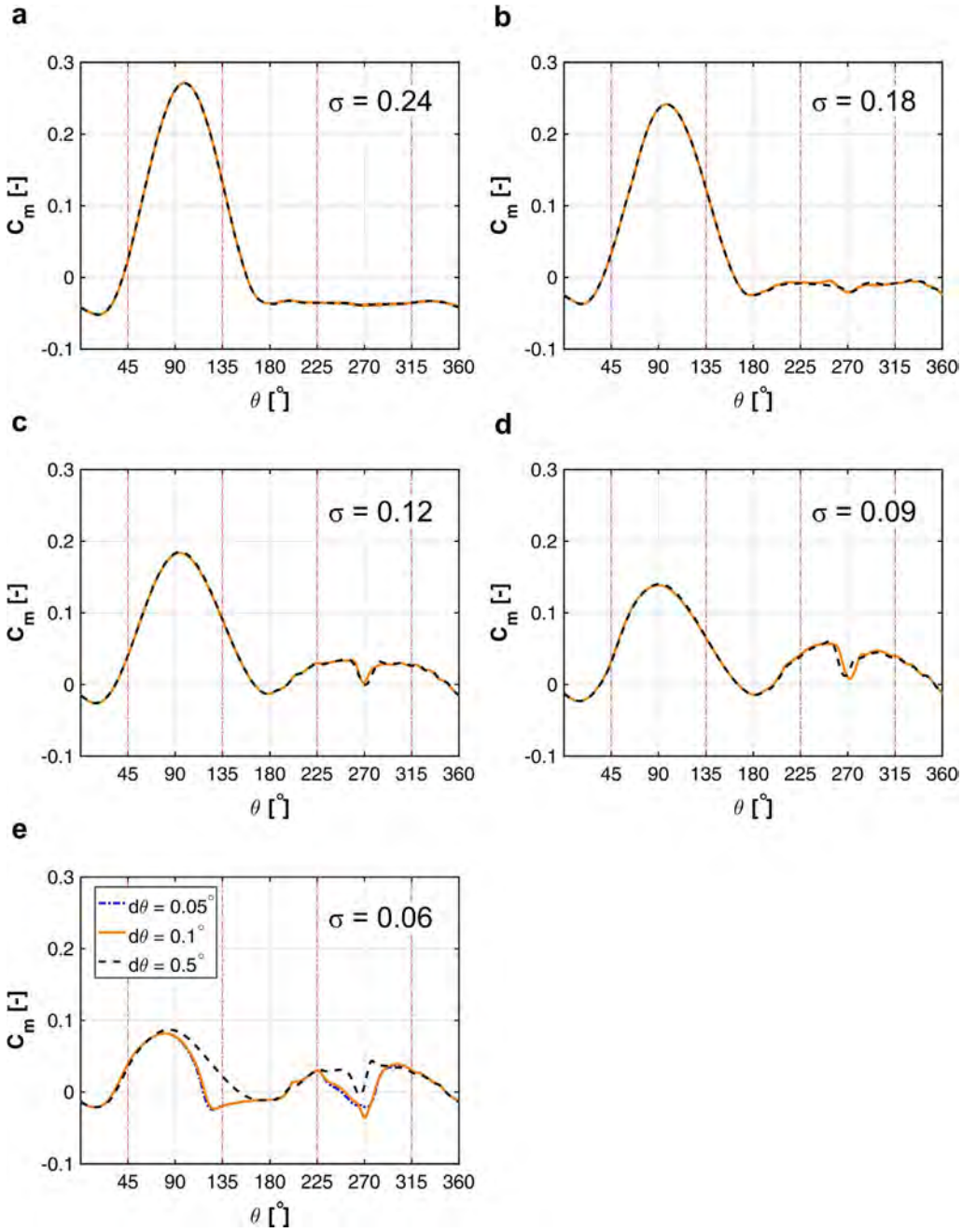

Fig. 7. Instantaneous moment coefficient for the last turbine revolution for different solidities using various azimuthal increments. (λ = 4.5).

(θ ≈ 270°) between the lines corresponding to dθ = 0.5° and dθ < 0.5° for σ = 0.09. However, this results in negligible (< 1%) difference in calculated C_P between the simulations with dθ = 0.5° and the finest dθ (0.05°) for 0.09 ≤ σ ≤ 0.24 (Fig. 8).

For a very low solidity of 0.06, significant differences in C_m (Fig. 7e) and C_P (Fig. 8) are observed for dθ = 0.5° and dθ < 0.5°. The difference in C_m is mainly apparent in two regions: 90° < θ < 160° and 225° < θ < 300° where the former is associated with the azimuthal angles where dynamic stall might occur, and the latter corresponds to the region where the consequent blade-wake interactions would happen (see Section 4.1).

Contours of instantaneous normalized lateral velocity at θ = 100° for turbines with solidities of 0.06 and 0.09 are presented in Fig. 9. The promotion of trailing edge separation and increase of the laminar separation bubble length due to lower Re_c for σ = 0.06 is clearly observed. This confirms that the observed deviation in C_m and C_P for σ = 0.06 is a result of the Reynolds number effect. Although at λ = 4.5 dynamic stall is avoided on the turbine blades (see Fig. 5b), the presence of strong Reynolds number effects could result in an earlier occurrence of stall on turbine blades at the same λ but lower chord-based Reynolds number Re_c [81]. The Re_c could be a result of the reduction in the airfoil chord length (which is equivalent to decrease in turbine solidity for a given n and D), which is also the case here. At λ = 4.5, Re_c for σ = 0.12 (c = 0.06 m) is 170 × 10^3 while this reduces to 80 × 10^3 for σ = 0.06. Therefore, regardless of tip speed ratio and solidity, low Reynolds number regime (Re_c < 10^5) would impose the finer minimum requirement of dθ = 0.1° to accurately predict the flow.

The impact of solidity on the minimum requirement for dθ is further investigated at a lower tip speed ratio of 2.5. The simulations are performed for dθ = 0.05° and 0.1°. The instantaneous moment coefficient C_m for the last turbine revolution versus azimuth θ is shown in Fig. 10. The comparison shows insignificant differences in C_P (< 1%) for dθ = 0.1°, which was shown to be the minimum requirement for dθ at such λ, and dθ = 0.05°. This means that in case the temporal resolution

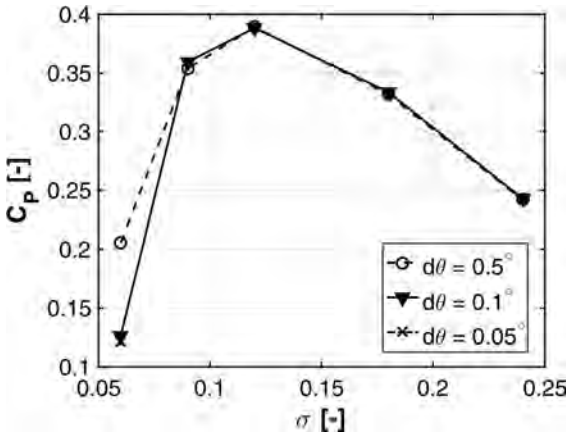

Fig. 8. Power coefficient for different solidities using various azimuthal increments. (λ = 4.5).

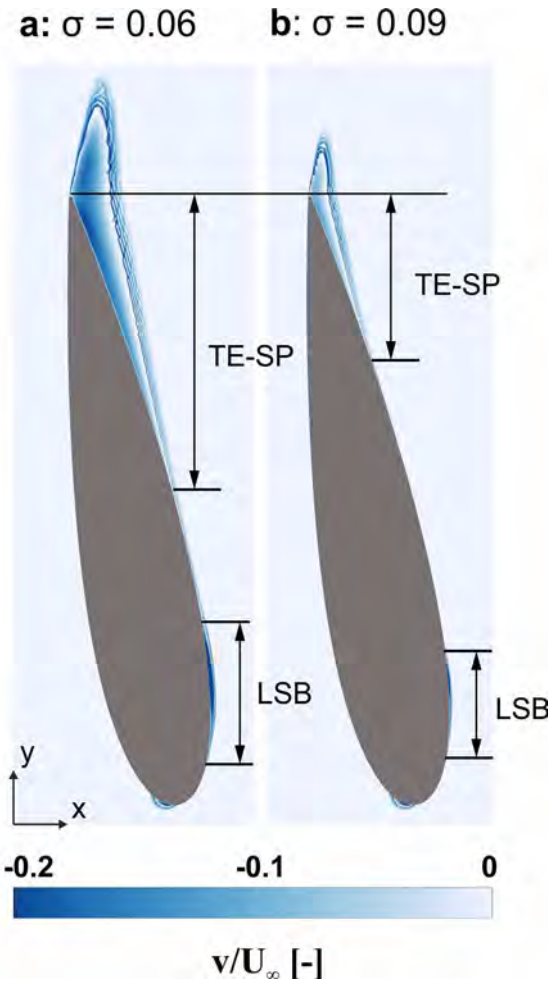

Fig. 9. Contour of instantaneous normalized lateral velocity at θ = 100° for turbines with solidities of (a) 0.06 and (b) 0.09 at λ = 4.5. (LSB: laminar separation bubble; TE-SP: trailing edge separation.)

of the simulation is adequate to accurately predict the dynamic stall and blade-wake interactions, the minimum requirement for dθ is independent of solidity at a given Re_c. Therefore, at a given Re_c, tip speed ratio remains the dominant parameter to set the minimum requirement for dθ while a low Re_c ($< 10^5$) might need the finer dθ of 0.1°.

It should be noted that in the current study, solidity is modified by changing the blade chord length, however, modifying the solidity by changing the number of blades would most likely have negligible effect on the provided minimum requirements for dθ. This is because changing the number of blades would neither affect Re_c nor the variations of angle of attack of the blades and consequently the dynamic stall behavior on blades while it only influences the frequency of occurrence of the blade-wake interactions. Nevertheless, more research is required to further investigate this.

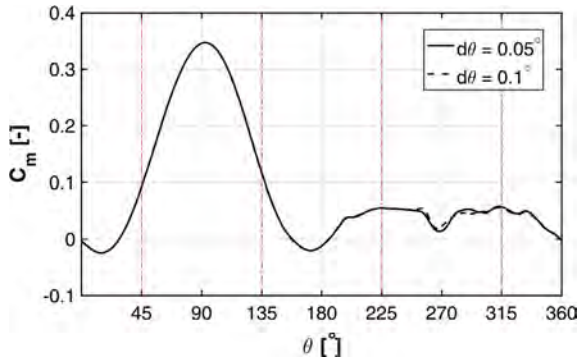

Fig. 10. Instantaneous moment coefficient for the last turbine revolution using different azimuthal increments (λ = 2.5, σ = 0.24).

5. Domain size: distance to the inlet

The operation of the turbine results in an induction field upstream of the turbine where the incoming flow is decelerated to lower velocities than the freestream. Rezaeiha et al. [6] showed that at λ = 4.5 and σ = 0.12 this induction field extends to more than 7.5D upstream. Therefore, the computational domain should extend far enough upstream not to cut this induction field. As the turbine induction field might change for different tip speed ratios and solidities, the dependency of the minimum requirement for the distance from the turbine center d_i to the inlet to λ and σ needs to be investigated. Note that the minimum requirements for domain width and the diameter of the rotating core are considered to be unaffected by the tip speed ratio and solidity (see Section 2.2). Dependency on distance to the outlet will be investigated in Section 6. A list of the main computational parameters of the cases investigated in the present section is given in Table 5.

5.1. Dependency on tip speed ratio

The instantaneous moment coefficient C_m for the last turbine revolution versus azimuth θ for tip speed ratios 2.5, 3.5 and 4.5 and for domains with different distance from the turbine center to the inlet $2.5D \leq d_i \leq 15D$ is shown in Fig. 11. The tip speed ratios are selected as typical moderately low and moderately high values relevant for VAWTs. The turbine solidity is 0.12, which is the same as the reference case. It is seen that the simulations using domains with $d_i < 10D$ overestimate C_m. This is more pronounced for higher tip speed ratios (Fig. 11a-b), especially during the upwind quartile $45° \leq \theta < 135°$. This is associated with cutting the induction field, which results in

Table 5
Description of cases for the study of distance to inlet.

d_i/D	d_o/D	Domain size (L/D) × (W/D)	dθ [°]	λ	σ
2.5	25	27.5 × 20	0.1	2.5, 3.5, 4.5†	0.12†, 0.24
5†	25†	30 × 20†	0.1†	2.5, 3.5, 4.5†	0.12†, 0.24
7.5	25	32.5 × 20	0.1	2.5, 3.5, 4.5†	0.12†, 0.24
10	25	35 × 20	0.1	2.5, 3.5, 4.5†	0.12†, 0.24
15	25	40 × 20	0.1	2.5, 3.5, 4.5†	0.12†, 0.24

Note: The reference case is shown with '†' sign.

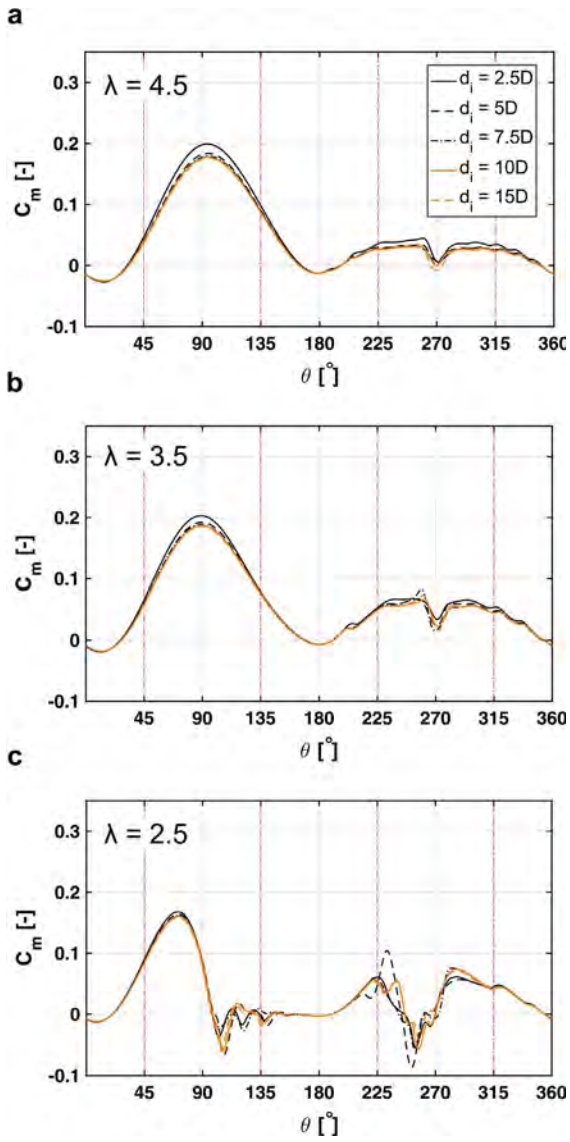

Fig. 11. The instantaneous moment coefficient during the last turbine revolution for tip speed ratios of (a) 4.5, (b) 3.5 and (c) 2.5 using domains with different d_i/D values. ($\sigma = 0.12$).

higher incoming velocity at the turbine incident and consequently higher C_m on blades. For higher values of d_i (10D and 15D), however, the C_m distribution is almost the same for all tip speed ratios.

Fig. 12 shows the difference between the predicted turbine C_P for different tip speed ratios calculated using domains with different d_i compared to the longest domain with $d_i = 15D$. Substantial differences can be observed for domains with $d_i < 15D$. The figure illustrates that $|\Delta C_P|$ increases when λ becomes larger. This shows that the solution is more sensitive to the domain size at higher λ values. The non-monotonic value of $|\Delta C_P|$ occurring for $\lambda = 2.5$ using domains with d_i of 5D and 7.5D could be attributed to some error cancellations in C_m curve. This suggests that comparison of the instantaneous values of C_m is more reliable than the averaged values of C_P for such an analysis.

The value of $|\Delta C_P|$ for domains with $d_i = 10D$ with respect to the domains with $d_i = 15D$ is 1.9% and 1.3% for $\lambda = 2.5$ and 4.5, respectively. The above discussions show that the minimum requirement for the distance from the turbine center to the domain inlet d_i in order to have $|\Delta C_P| < 1\%$ is 15D regardless of the turbine tip speed ratio.

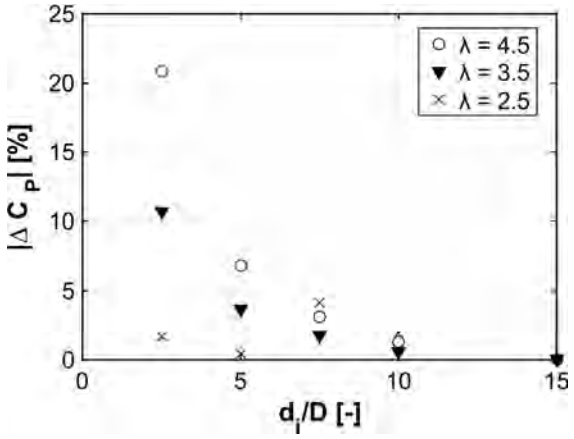

Fig. 12. The change in power coefficient (with respect to the domain with $d_i = 15D$) for various tip speed ratios using domains with different d_i/D values. ($\sigma = 0.12$).

5.2. Dependency on solidity

The instantaneous moment coefficient C_m for the last turbine revolution versus azimuth θ for solidity of 0.12 and 0.24 calculated using domains with different distance from the turbine center to the inlet $5D \le d_i \le 15D$ is shown in Fig. 13. The solidities are selected as two typical moderately low and moderately high values relevant for VAWTs. The tip speed ratio is 4.5, which is the same as the reference case. Note that to reduce the computational cost, the $d_i = 2.5D$ is no longer considered as the minimum distance as used in Section 5.1 as it was already shown to be too small. It can be seen that the simulations using domains with $d_i < 10D$ overestimate C_m compared to the domains with $d_i \ge 10D$. This is more significant for solidity of 0.24 (Fig. 13b) and during the upwind quartile ($45° \le \theta < 135°$). Similarly, the observed overestimation of C_m for domains with $d_i < 10D$ is attributed to cutting the turbine upstream induction field. For higher values of d_i, the differences are negligible.

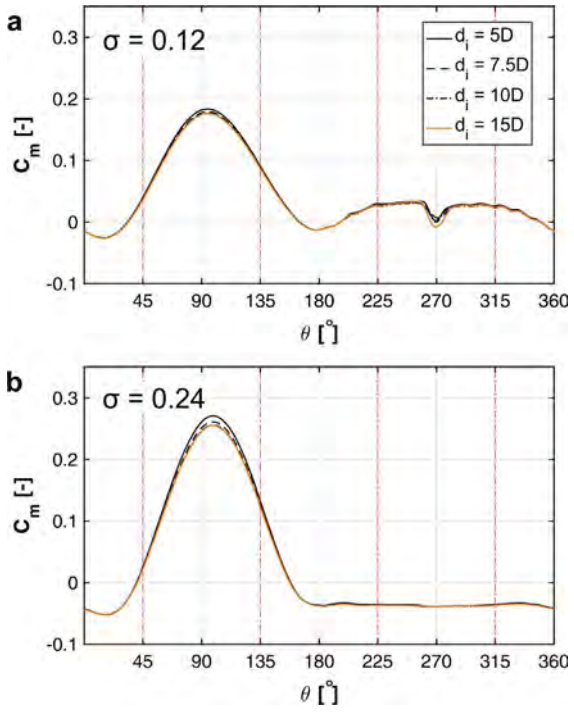

Fig. 13. The instantaneous moment coefficient during the last turbine revolution for solidities of (a) 0.12 and (b) 0.24 using domains with different d_i values. ($\lambda = 4.5$).

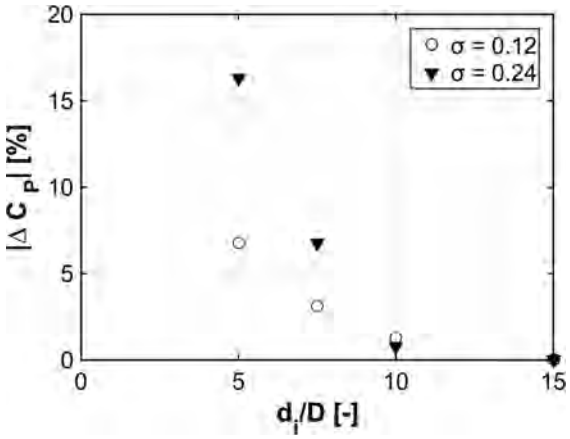

Fig. 14. The change in power coefficient (with respect to the domain with d_i = 15D) for various solidities using domains with different d_i. (λ = 4.5).

Fig. 14 shows the difference between the predicted turbine C_P for different solidities calculated using domains with different d_i values compared to the widest domain with d_i = 15D. Significant differences can be observed for domains with $d_i \leq$ 10D. This is in line with the trend observed for C_m in Fig. 13. The figure illustrates that C_m variations with domain size increases when σ becomes larger. This shows that the solution is more sensitive to the domain size at higher σ values.

The observations above conclude that the derived minimum requirement for d_i in Section 5.1, i.e. d_i = 15D, is valid regardless of the turbine solidity. This value will ensure that the predicted turbine performance, at different tip speed ratios and solidities, is minimally affected by d_i and the domain sufficiently contains the induction field upstream of the turbine.

6. Domain size: distance to the outlet

The operation of the turbine results in the generation of a wake downstream of the turbine where the flow has lower velocity and higher turbulence intensity than the freestream. Rezaeiha et al. [6] showed that at λ = 4.5 and σ = 0.12, the turbine C_P is underpredicted with more than 2% for domains with $d_o <$ 10D, where d_o is the distance from the turbine center to the domain outlet. Therefore, the computational domain should extend far enough downstream to allow the turbine wake to sufficiently develop. As the turbine wake length might alter for different tip speed ratios and solidities [82], a systematic analysis of the minimum requirement for d_o for different tip speed ratios and solidities is needed. A list of the main computational parameters of the cases investigated in the present section is given in Table 6.

6.1. Dependency on tip speed ratio

Fig. 15 presents the instantaneous moment coefficient C_m for the last turbine revolution versus azimuth θ for tip speed ratios of 2.5, 3.5 and 4.5 obtained using domains with different distance from the turbine center to the outlet 6D $\leq d_o \leq$ 55D. Fig. 16 shows the difference between the C_P for different tip speed ratios calculated using domains with different d_o compared to the longest domain, i.e. d_o = 55D. Note that two tip speed ratios are selected as typical moderately low and moderately high values relevant for VAWTs. The turbine solidity is 0.12, which is the same as the reference case. It can be seen that for all λ values the sensitivity of C_m to d_o is considerably less compared to that observed for d_i. In addition, Fig. 15 illustrates that C_m variations with domain size increases when λ becomes larger. In the downwind quartile (225° $\leq \theta <$ 315°), a small difference between the results of the domains with $d_o <$ 10D and domains with $d_o \geq$ 10D is observed. This results in 2.2% deviation in the predicted C_p using domains with d_o = 6D and d_o = 55D for λ = 4.5 (Fig. 16). Moreover, Fig. 16 also exhibits higher $|\Delta C_P|$ values when λ becomes larger. This shows that the solution is more sensitive to the domain size at higher λ. Note that a similar trend was also observed for d_i (see Section 5.1). For all the studied tip speed ratios, the difference between the predicted turbine C_P using the domains with $d_o \geq$ 10D and the domain with d_o = 55D is less than 1%. Therefore, d_o = 10D is considered as the minimum requirement for d_o regardless of the tip speed ratio.

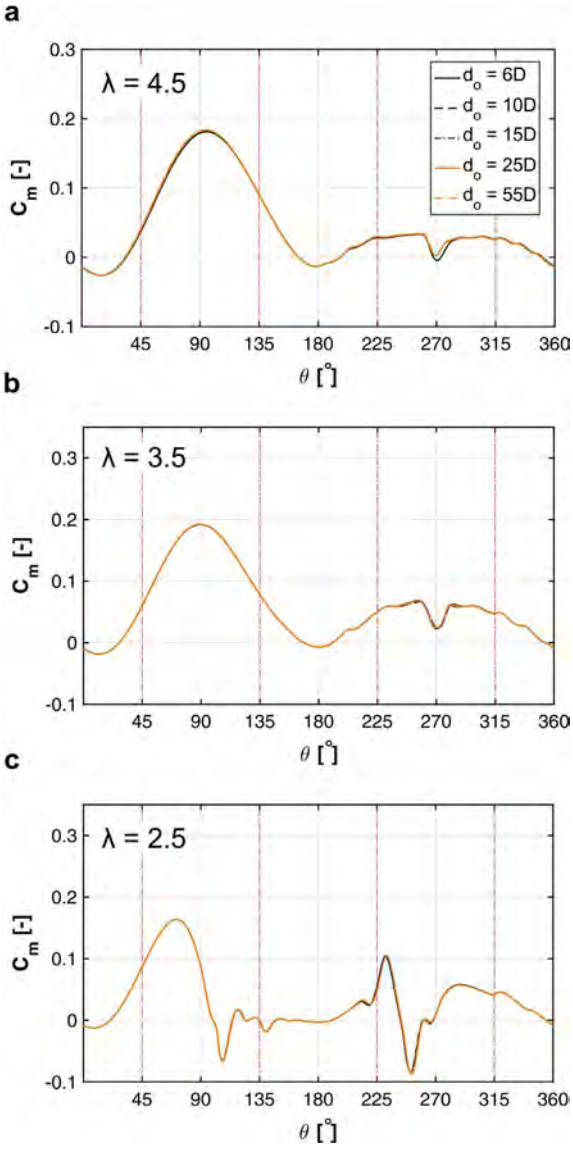

Fig. 15. The instantaneous moment coefficient during the last turbine revolution for tip speed ratios of (a) 4.5, (b) 3.5 and (c) 2.5 using domains with different d_o/D values. (σ = 0.12).

Table 6
Description of cases for the study of distance to outlet.

d_i/D	d_o/D	Domain size (L/D) × (W/D)	dθ [°]	λ	σ
5	6	11 × 20	0.1	2.5, 3.5, 4.5†	0.12†, 0.24
5	10	15 × 20	0.1	2.5, 3.5, 4.5†	0.12†, 0.24
5	15	20 × 20	0.1	2.5, 3.5, 4.5†	0.12†, 0.24
5†	25†	30 × 20†	0.1†	2.5, 3.5, 4.5†	0.12†, 0.24
5	55	60 × 20	0.1	2.5, 3.5, 4.5†	0.12†, 0.24

Note: The reference case is shown with '†' sign.

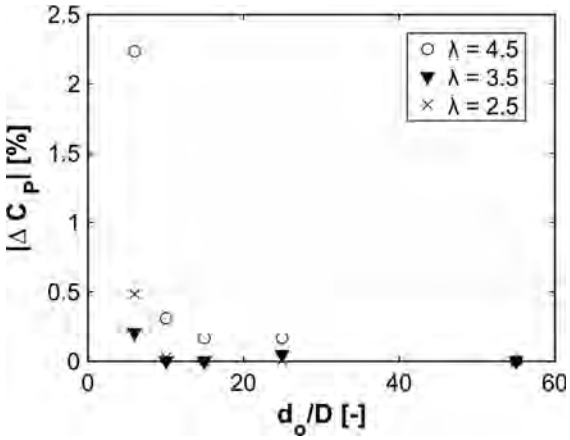

Fig. 16. The change in power coefficient (with respect to the domain with d_o = 55D) for various tip speed ratios using domains with different d_o/D values. (σ = 0.12).

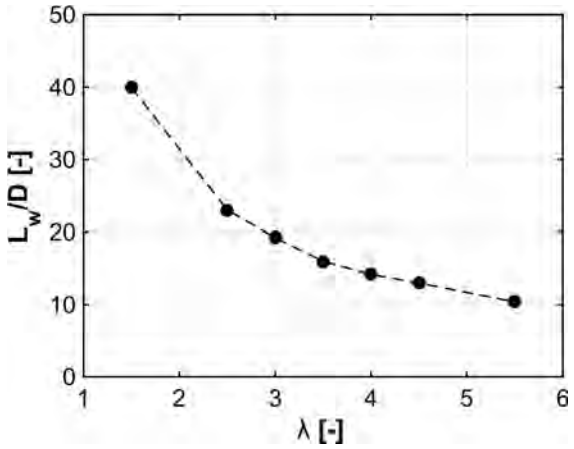

Fig. 18. Length of the turbine wake versus tip speed ratio.

Contours of the normalized velocity magnitude illustrating the turbine wake for different tip speed ratios are shown in Fig. 17. The length of the turbine wake, defined as the length in which $U/U_\infty = 0.97$, as a function of tip speed ratio (σ = 0.12) is presented in Fig. 18. The two figures imply that the CFD results could still be sufficiently accurate, though the computational domain might partially cut the turbine wake at $x/D \geq 10$. This could be associated with strong velocity gradients occurring at $x/D < 10$, which is most particularly observed for higher λ values. This also explains the higher sensitivity of the predicted turbine C_m (Fig. 15a) and $|\Delta C_p|$ (Fig. 16) to d_o for high λ values.

The decrease in the turbine wake length with increasing λ was already observed for horizontal axis wind turbines [82]. The detailed analysis in Ref. [82] has shown that by increasing λ the distance between the shed vortices in the wake decreases, which leads to amplification of instabilities in the wake. This eventually leads to an earlier breakdown of the wake structure. Contours of instantaneous normalized lateral velocity for two tip speed ratio of 3.5 and 5.5 are shown in Fig. 19. The figure illustrates the trace of the blades' wake (dashed line) and the shed vortices from the blades on the leeward region traveling downstream (dotted circles). Two adjacent zones with different signs for lateral velocity are used to qualitatively identify the shed vortices. A comparison of Fig. 19a and b shows that the relative distance between the dashed lines and the center of the dotted circles has significantly increased for λ = 5.5 suggesting that the aforementioned mechanism is responsible for the reduction in the VAWT wake length by increasing λ.

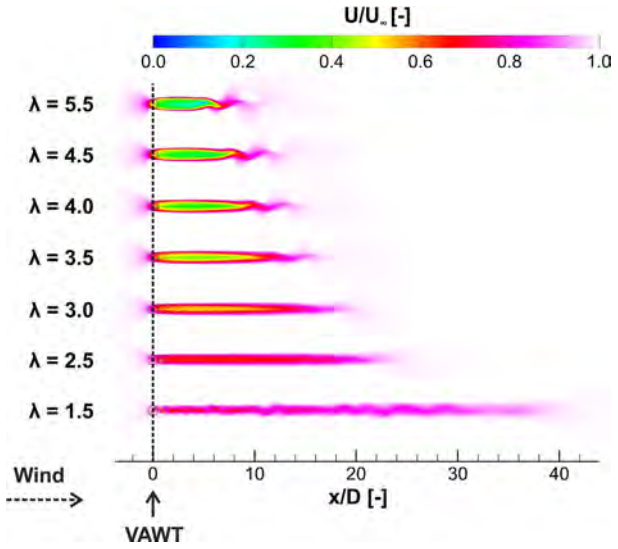

Fig. 17. Contours of instantaneous normalized velocity magnitude illustrating the turbine wake for different tip speed ratios.

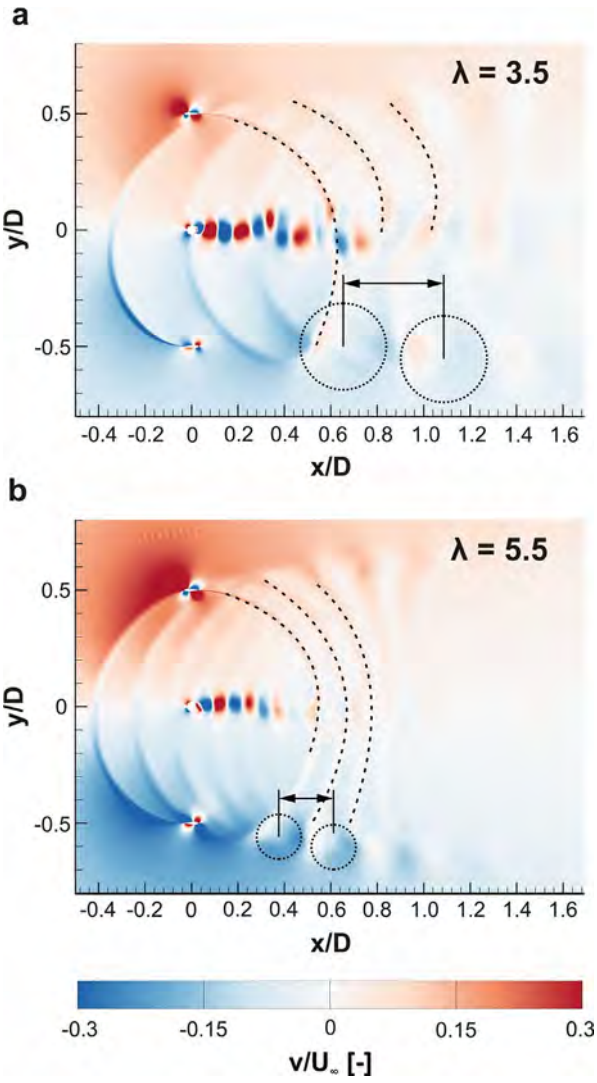

Fig. 19. Contours of instantaneous normalized lateral velocity in the near wake of the turbine for tip speed ratios of (a) 3.5 and (b) 5.5.

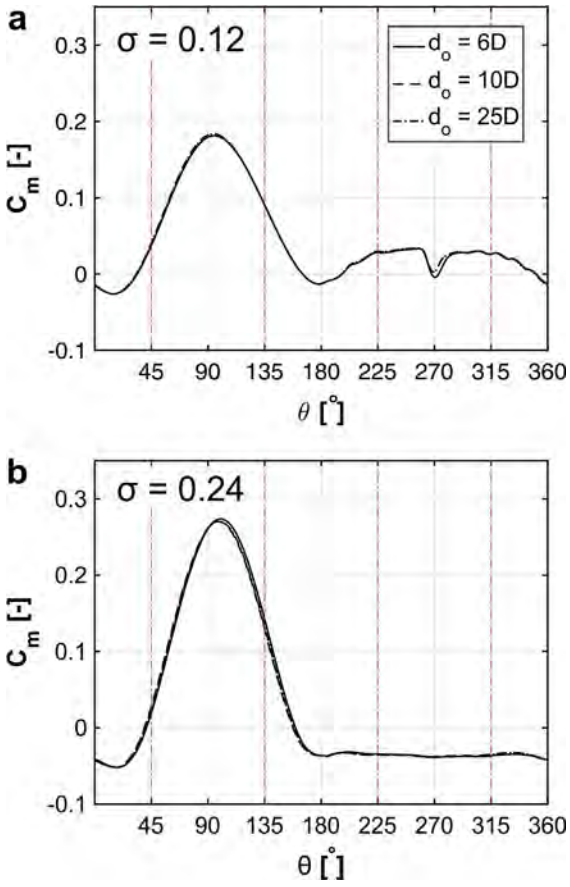

Fig. 20. The instantaneous moment coefficient during the last turbine revolution for solidities of (a) 0.12 and (b) 0.24 using domains with different d_o values ($\lambda = 4.5$).

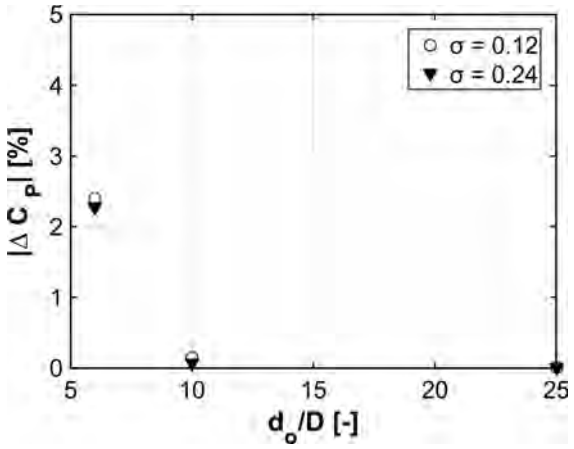

Fig. 21. The change in power coefficient (with respect to the domain with d_o = 25D) for various solidities using domains with different d_o ($\lambda = 4.5$).

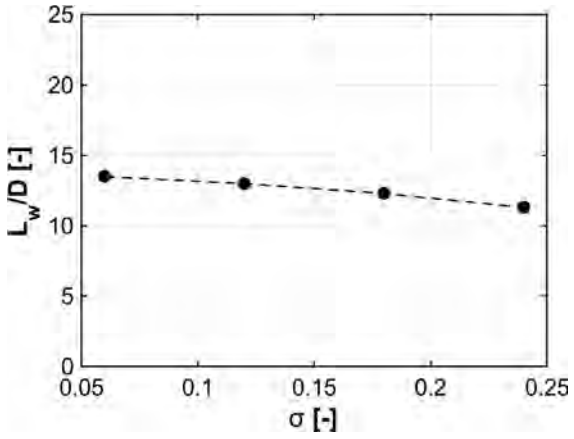

Fig. 22. Length of the turbine wake versus solidity.

6.2. Dependency on solidity

The instantaneous moment coefficient C_m for the last turbine revolution versus azimuth θ for solidities of 0.12 and 0.24 calculated using domains with different distance from the turbine center to the outlet $6D \leq d_o \leq 25D$ is shown in Fig. 20. The difference between the predicted turbine C_P for different solidities calculated using domains with different d_o compared to the longest domain with $d_o = 25D$ is shown in Fig. 21. The solidities are selected as two typical moderately low and moderately high values relevant for VAWTs. The tip speed ratio is 4.5, which is the same as the reference case. Note that to reduce the computational cost, the case with $d_o = 55D$ is no longer considered because the minimum requirement derived in Section 6.1 is 10D and $d_o = 55D$ is already predicted to be too large. It can be seen that there is an observable difference in C_m between the values calculated using domains with $d_o < 10D$ and $d_o \geq 10D$ while the lines corresponding to $d_o = 10D$ and 25D overlap. This difference results in 2.3% deviation between the calculated C_P using domains with d_o of 6D and 25D while this deviation is less than 1% for domains with d_o of 10D and 25D (Fig. 21). Therefore, the already derived minimum requirement for d_o (in Section 6.1) can also be employed regardless of the turbine solidity. This value ($d_o = 10D$) will ensure that the predicted turbine performance, at different tip speed ratios and solidities, is not significantly affected by d_o and the domain sufficiently allows the turbine wake to develop so that cutting the wake will have < 1% effect of the predicted turbine C_P.

The turbine wake length as a function of solidity at $\lambda = 4.5$ is shown in Fig. 22. As already discussed in Section 6.1, partial cutting of the wake at $d_o \geq 10D$ will have < 1% effect on the predicted turbine performance.

A similar explanation can be presented for the decrease in the wake length with increasing solidity. Increasing solidity (with increasing the blade chord length) will lead to increase in the length scale of the shed vortices in the turbine wake, which leads to the smaller relative distance between the vortices at the given λ. This will amplify the instabilities in the wake and eventually will result in the earlier breakdown of the wake structure. A comparison of the trends observed in Fig. 22 and Fig. 18 implies that the length of the turbine wake is more sensitive to tip speed ratio than the solidity.

7. Convergence criterion

For transient simulations, it is importance to initiate the data sampling only after the solution has reached a statistically steady state condition. For the case of wind turbines, it is customary to correlate the convergence of the unsteady simulation with the turbine revolution and to express it as the minimum number of turbine revolutions that the simulations needs to continue before reaching a statistically steady state condition. Fig. 23 schematically presents the definition of the statistical steady state condition employed in the present study. As the complexity of the flow for VAWTs varies with the operating and geometrical conditions, i.e. λ and σ, therefore, a sensitivity analysis is performed for the convergence criterion by applying systematic changes to the reference case. In this section, the sensitivity of the minimum requirements for the convergence criterion to different tip speed ratios and solidities are investigated. The details of the main computational parameters of the cases that are investigated are presented in Table 7.

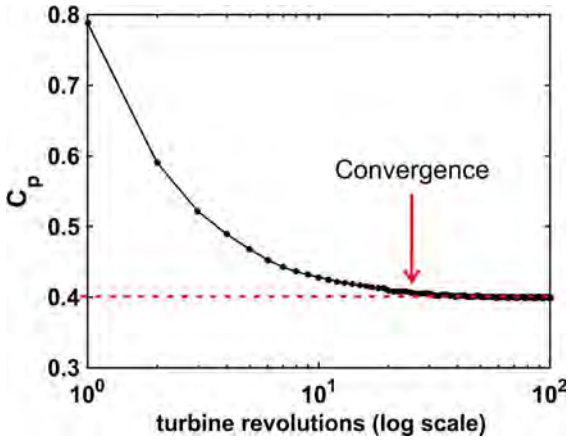

Fig. 23. Schematic of the time history of C_P versus turbine revolutions along with the statistical steady state condition used in the present study.

Table 7
Description of cases for the study of convergence criterion.

d_i/D	d_o/D	Domain size (L/D) × (W/D)	dθ [°]	λ	σ	# turbine revolutions
5†	25†	30 × 20†	0.1†	2.5, 4.5†	0.12†, 0.24	50

Note: The reference case is shown with '†' sign.

7.1. Dependency on tip speed ratio

The convergence of the results as a function of the turbine revolution is studied for different tip speed ratios. Fig. 24 shows the time history of C_P during 50 turbine revolutions for two different tip speed ratio of 2.5 and 4.5. The tip speed ratios are selected as typical moderately low and moderately high values relevant for VAWTs. The turbine solidity is 0.12, which is the same as the reference case. It can be seen that after 20 turbine revolutions a statistically steady state condition is observed for all cases, as the C_P variation with respect to 50th revolution has become < 2%. The difference in C_P between two subsequent changes at 20 revolutions onwards is less than 0.2%. This is in line with the results of the earlier study by Rezaeiha et al. [6], which shows that 20–30 turbine revolutions is sufficient as the convergence criterion for a moderate tip speed ratio of 4.5 with a low solidity of 0.12. The results of the present study confirm that this convergence criterion can be generalized for other tip speed ratios. This suggests that 20–30 turbine revolutions are sufficient to allow the development of the flow over a VAWT so that statistically steady results are obtained irrespective of tip speed ratio. Note that at low tip speed ratios due to the inherent three-dimensional flow complexities associated to dynamic stall on blades and blade-wake interactions and the limitations of 2D modeling, the calculated C_P might have some small oscillations between the subsequent turbine revolutions. Nevertheless, after approximately 20th revolution, the difference between the C_P, for λ = 2.5, obtained after 20 revolutions and that after 50 revolutions remains below 2%.

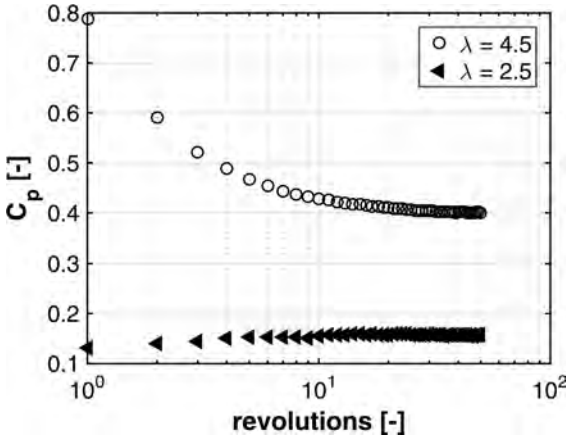

Fig. 24. Time history of power coefficient for 50 turbine revolutions for different tip speed ratios in log-scale. (σ = 0.12).

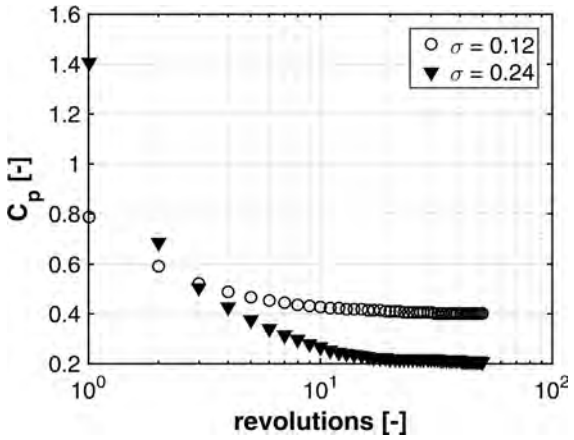

Fig. 25. Time history of power coefficient for 50 turbine revolutions for solidities in log-scale. (λ = 4.5).

7.2. Dependency on solidity

The convergence of the results as a function of the turbine revolution is studied for different solidities. Fig. 25 shows the time history of power coefficient C_P during 50 turbine revolutions for two different solidities of 0.12 and 0.24. The solidities are selected as two typical moderately low and moderately high values relevant for VAWTs. The tip speed ratio is 4.5, which is the same as the reference case. It can be seen that after 20 turbine revolutions a statistically steady state solution is observed for all cases, as the C_P variations with respect to 50th revolution is negligible (< 2%). The difference in C_P between two subsequent changes at 20 revolutions onwards is less than 0.2%. The results of the present study confirm that this convergence criterion can be generalized for other solidities. This suggests that 20–30 turbine revolutions are sufficient to allow the development of the flow over a VAWT so that statistically steady state results are obtained for the two studied cases with moderately low and moderately high solidities.

8. Discussion

The provided guidelines have been prepared using 110 high-fidelity CFD simulations each running for approximately 120 h on 24 cores on the Dutch national supercomputer SURFSARA, Cartesius (www.surfsara.nl). This corresponds to approximately 320,000 CPU hours. In total, a wide range of operational ($1.5 \le \lambda \le 5.5$), geometrical ($0.12 \le \sigma \le 0.24$) and computational parameters ($0.025^\circ \le d\theta \le 0.5^\circ$; $2.5D \le d_i \le 15D$; $6D \le d_o \le 55D$; number of turbine revolutions ≤50) were studied. This is to strengthen the general character of the guidelines.

The CFD simulations are based on two validation studies with wind tunnel measurements. Note that the presented validation study is performed using the very fine dθ of 0.1°, which is finer than (or equal to) the derived minimum requirements for all λ values.

The minimum requirements are derived based on limiting the effect of each studied parameter (azimuthal increment, distance from turbine center to domain inlet and outlet and number of turbine revolutions) on turbine C_P to less than 1%. However, one should note that this does not mean that the total error of the CFD simulation associated with such computational parameters is 1%. A simple numerical error analysis

would reveal that the aforementioned errors can sum up to higher values which together with the other numerical errors; i.e. physical approximation error (e.g. 2D assumption as a representative of the turbine mid-plane), round-off error, iterative convergence error, spatial discretization error; would propagate to the final predicted turbine C_P. Therefore, one should not underestimate the importance of such minimum requirements to minimize the numerical error.

On the other hand, the findings of this study are limited to URANS simulations. For scale-resolving simulations (SRS), such as hybrid RANS-LES and LES, different requirements, specifically for convergence criterion and azimuthal increment, would be necessary which demands further investigation. Moreover, for SRS, the difference between consecutive turbine revolutions would be significant which, therefore, C_m and C_P values would need to be averaged over multiple turbine revolutions to be a representative of the turbine averaged performance. The number of turbine revolutions for such averaging would require a dedicated study.

In the current study, solidity was modified by changing the blade chord length at a given number of blades (n = 2). Although the provided minimum requirements are most likely not affected by the number of blades, a detailed investigation of that is proposed for future research.

Moreover, chord-based Reynolds number Re_c was also found to be influential for determination of dθ. Therefore, a dedicated investigation of the impact of Re_c on the provided minimum requirements for dθ is proposed for future research.

9. Conclusions

A systematic sensitivity analysis is performed using URANS simulations to provide the minimum requirements for azimuthal increment, domain size and convergence criterion for CFD simulation of VAWTs at different tip speed ratios and solidities. The evaluation is based on validation with wind-tunnel measurements for two VAWTs. The following conclusions are obtained:

(1) Azimuthal increment:

The minimum requirement for azimuthal increment is significantly dependent on the flow regime over the turbine blades. As the variations of the angle of attack of the turbine blades are mainly driven by the tip speed ratio, this parameter is the dominant factor to set the minimum requirements for azimuthal increment. The derived minimum requirements for azimuthal increment are:

- Low to moderate tip speed ratios: $d\theta = 0.1^\circ$
- Moderate to high tip speed ratios: $d\theta = 0.5^\circ$

These values will ensure that the flow complexities such as dynamic stall and blade-wake interactions are accurately predicted. For the studied turbine with a solidity of 0.12, the former regime corresponds to $1.5 \leq \lambda \leq 3.5$ while the latter refers to $3.5 < \lambda \leq 5.5$. In general, the low to moderate tip speed ratio regime corresponds to the region where the variations of the angle of attack of the blades exceed the static stall angle and dynamic stall and the blade-wake interactions are thus present. Conversely, the moderate to high tip speed ratios correspond to the regime where the variations of the angle of attack of the blade are below static stall angle, and the flow is mostly attached. Therefore, one should have a prior knowledge of the following two important factors to distinguish between the aforementioned operating regimes of tip speed ratio:

- Variations of the angle of attack for the operating regime of the turbine to be studied.
- Static stall angle of the employed airfoil on the turbine blade.

In addition, it is important to note that any change in geometrical and operational characteristics of the turbine which could induce a different flow separation behavior over the blades would require the finer dθ of 0.1°. The change in geometrical parameters includes, but not limited to:

- Changing the airfoil shape
- Changing the blade chord length (solidity)
- Changing the blade surface roughness
- Introducing pitch angle to blade
- Adding passive/active flow control devices on blades.

The change in operating conditions includes operating the turbine at:

- Low chord-based Reynolds number ($Re_c < 10^5$)
- Low freestream turbulence intensity (TI < 5%)

Therefore, for any reason, if a user is not certain of the regime of tip speed ratio of the turbine, an azimuthal increment of 0.1° is always the safe choice to be employed for URANS simulations of VAWTs.

(2) Domain size:

The minimum distance from the turbine center to the domain inlet needs to be 15D. This can be a safe choice to let the domain sufficiently contain the turbine upstream induction field regardless of the tip speed ratio and solidity.

The minimum distance from the turbine center to the domain outlet needs to be 10D. This value will ensure that the turbine wake is sufficiently developed inside the domain so that it allows accurate prediction of the turbine performance regardless of the tip speed ratio and solidity.

(3) Convergence:

The minimum number of turbine revolutions to ensure that the simulations have reached a statistically steady state condition is 20–30 turbine revolutions. This convergence criterion can be employed regardless of tip speed ratio and solidity.

The aforementioned minimum requirements can be employed as guidelines to ensure the accuracy of CFD simulation of VAWTs.

Acknowledgement

The authors would like to acknowledge support from the European Commission's Framework Program Horizon 2020, through the Marie Curie Innovative Training Network (ITN) AEOLUS4FUTURE - Efficient harvesting of the wind energy (H2020-MSCA-ITN-2014: Grant agreement no. 643167) and the TU1304 COST ACTION “WINERCOST”. The authors gratefully acknowledge the partnership with ANSYS CFD. This work was sponsored by NWO Exacte Wetenschappen (Physical Sciences) for the use of supercomputer facilities, with financial support from the Nederlandse Organisatie voor Wetenschappelijk Onderzoek (Netherlands Organization for Scientific Research, NWO). The 2nd author, Hamid Montazeri, is currently a postdoctoral fellow of the Research Foundation – Flanders (FWO) and is grateful for its financial support (project FWO 12M5316N).

References

[1] Bedon G, Schmidt Paulsen U, Aagaard Madsen H, Belloni F, Raciti Castelli M, Benini E. Computational assessment of the DeepWind aerodynamic performance with different blade and airfoil configurations. Appl Energy 2017;185(2):1100–8.
[2] Qa Li, Kamada Y, Maeda T, Murata J, Okumura Y. Fundamental study on aerodynamic force of floating offshore wind turbine with cyclic pitch mechanism. Energy 2016;99:20–31.

[3] Tummala A, Velamati RK, Sinha DK, Indraja V, Krishna VH. A review on small scale wind turbines. Renew Sustain Energy Rev 2016;56:1351–71.
[4] Gsänger S, Pitteloud JD. Small wind world report summary. World Wind Energy Association (WWEA); 2015.
[5] Toja-Silva F, Colmenar-Santos A, Castro-Gil M. Urban wind energy exploitation systems: behaviour under multidirectional flow conditions—opportunities and challenges. Renew Sustain Energy Rev 2013;24:364–78.
[6] Rezaeiha A, Kalkman I, Blocken B. CFD simulation of a vertical axis wind turbine operating at a moderate tip speed ratio: guidelines for minimum domain size and azimuthal increment. Renew Energy 2017;107:373–85.
[7] Rezaeiha A, Pereira R, Kotsonis M. Fluctuations of angle of attack and lift coefficient and the resultant fatigue loads for a large horizontal axis wind turbine. Renew Energy 2017;114(B):904–16.
[8] Simão Ferreira C, van Kuik G, van Bussel G, Scarano F. Visualization by PIV of dynamic stall on a vertical axis wind turbine. Exp Fluids 2008;46(1):97–108.
[9] Yu JM, Leu TS, Miau JJ. Investigation of reduced frequency and freestream turbulence effects on dynamic stall of a pitching airfoil. J Visual 2017;20(1):31–44.
[10] Amet E, Maître T, Pellone C, Achard JL. 2D numerical simulations of blade-vortex interaction in a Darrieus turbine. J Fluids Eng 2009;131(11). 111103(1-15).
[11] Bianchini A, Balduzzi F, Rainbird JM, Peiro J, Graham JMR, Ferrara G, et al. An experimental and numerical assessment of airfoil polars for use in Darrieus wind turbines—part I: flow curvature effects. J Eng Gas Turbines Power 2015;138(032602).
[12] Bianchini A, Balduzzi F, Ferrara G, Ferrari L. Virtual incidence effect on rotating airfoils in Darrieus wind turbines. Energy Convers Manage 2016;111:329–38.
[13] Simão Ferreira C, Madsen HA, Barone M, Roscher B, Deglaire P, Arduin I. Comparison of aerodynamic models for vertical axis wind turbines. J Phys: Conf Ser 2014;524(012125).
[14] Bianchini A, Balduzzi F, Bachant P, Ferrara G, Ferrari L. Effectiveness of two-dimensional CFD simulations for Darrieus VAWTs: a combined numerical and experimental assessment. Energy Convers Manage 2017;136:318–28.
[15] Bianchini A, Balduzzi F, Ferrara G, Ferrari L. A computational procedure to define the incidence angle on airfoils rotating around an axis orthogonal to flow direction. Energy Convers Manage 2016;126:790–8.
[16] Ghasemian M, Ashrafi ZN, Sedaghat A. A review on computational fluid dynamic simulation techniques for Darrieus vertical axis wind turbines. Energy Convers Manage 2017;149:87–100.
[17] Lei H, Zhou D, Bao Y, Li Y, Han Z. Three-dimensional Improved Delayed Detached Eddy Simulation of a two-bladed vertical axis wind turbine. Energy Convers Manage 2017;133:235–48.
[18] Shen X, Yang H, Chen J, Zhu X, Du Z. Aerodynamic shape optimization of non-straight small wind turbine blades. Energy Convers Manage 2016;119:266–78.
[19] Tahani M, Babayan N, Mehrnia S, Shadmehri M. A novel heuristic method for optimization of straight blade vertical axis wind turbine. Energy Convers Manage 2016;127:461–76.
[20] Blocken B. 50 years of computational wind engineering: past, present and future. J Wind Eng Ind Aerodyn 2014;129:69–102.
[21] Rezaeiha A, Montazeri H, and Blocken B. CFD simulations of vertical axis wind turbines: impact of turbulence modeling; 2018 [in preparation].
[22] Araya DB, Colonius T, Dabiri JO. Transition to bluff-body dynamics in the wake of vertical-axis wind turbines. J Fluid Mech 2017;813:346–81.
[23] Abkar M, Dabiri JO. Self-similarity and flow characteristics of vertical-axis wind turbine wakes: an LES study. J Turbul 2017;18(4):373–89.
[24] Ryan KJ, Coletti F, Elkins CJ, Dabiri JO, Eaton JK. Three-dimensional flow field around and downstream of a subscale model rotating vertical axis wind turbine. Exp Fluids 2016;57(3).
[25] Kinzel M, Araya DB, Dabiri JO. Turbulence in vertical axis wind turbine canopies. Phys Fluids 2015;27(11):115102.
[26] Tescione G, Ragni D, He C, Simão Ferreira C, van Bussel GJW. Near wake flow analysis of a vertical axis wind turbine by stereoscopic particle image velocimetry. Renew Energy 2014;70:47–61.
[27] Simão Ferreira C, Scheurich F. Demonstrating that power and instantaneous loads are decoupled in a vertical-axis wind turbine. Wind Energy 2014;17(3):385–96.
[28] Qa Li, Maeda T, Kamada Y, Murata J, Furukawa K, Yamamoto M. Effect of number of blades on aerodynamic forces on a straight-bladed Vertical Axis Wind Turbine. Energy 2015;90:784–95.
[29] Li Q, Maeda T, Kamada Y, Shimizu K, Ogasawara T, Nakai A, et al. Effect of rotor aspect ratio and solidity on a straight-bladed vertical axis wind turbine in three-dimensional analysis by the panel method. Energy 2017;121:1–9.
[30] Subramanian A, Yogesh SA, Sivanandan H, Giri A, Vasudevan M, Mugundhan V, et al. Effect of airfoil and solidity on performance of small scale vertical axis wind turbine using three dimensional CFD model. Energy 2017;133:179–90.
[31] Simão Ferreira C, Geurts B. Aerofoil optimization for vertical-axis wind turbines. Wind Energy 2014;18(8):1371–85.
[32] Ragni D, Simão Ferreira C, Correale G. Experimental investigation of an optimized airfoil for vertical-axis wind turbines. Wind Energy 2014;18(9):1629–43.
[33] Rezaeiha A, Montazeri H, and Blocken B. Effect of airfoil shape on aerodynamic performance of vertical axis wind turbines; 2018 [in preparation].
[34] Rezaeiha A, Montazeri H, Blocken B. Characterization of aerodynamic performance of vertical axis wind turbines: impact of geometrical parameters; 2018 [in preparation].
[35] Bausas MD, Danao LAM. The aerodynamics of a camber-bladed vertical axis wind turbine in unsteady wind. Energy 2015;93:1155–64.
[36] Peng HY, Lam HF. Turbulence effects on the wake characteristics and aerodynamic performance of a straight-bladed vertical axis wind turbine by wind tunnel tests and large eddy simulations. Energy 2016;109:557–68.
[37] Qa Li, Maeda T, Kamada Y, Murata J, Furukawa K, Yamamoto M. The influence of flow field and aerodynamic forces on a straight-bladed vertical axis wind turbine. Energy 2016;111:260–71.
[38] Rezaeiha A, Montazeri H, Blocken B. Characterization of aerodynamic performance of vertical axis wind turbines: impact of operational parameters; 2018 [submitted for publication].
[39] Rezaeiha A, Kalkman I, Blocken B. Effect of pitch angle on power performance and aerodynamics of a vertical axis wind turbine. Appl Energy 2017;197:132–50.
[40] Rezaeiha A, Kalkman I, Montazeri H, Blocken B. Effect of the shaft on the aerodynamic performance of urban vertical axis wind turbines. Energy Convers Manage 2017;149(C):616–30.
[41] Wong KH, Chong WT, Sukiman NL, Poh SC, Shiah Y-C, Wang C-T. Performance enhancements on vertical axis wind turbines using flow augmentation systems: a review. Renew Sustain Energy Rev 2017;73:904–21.
[42] Scungio M, Arpino F, Focanti V, Profili M, Rotondi M. Wind tunnel testing of scaled models of a newly developed Darrieus-style vertical axis wind turbine with auxiliary straight blades. Energy Convers Manage 2016;130:60–70.
[43] Shahizare B, Nik-Ghazali N, Chong WT, Tabatabaeikia S, Izadyar N, Esmaeilzadeh A. Novel investigation of the different Omni-direction-guide-vane angles effects on the urban vertical axis wind turbine output power via three-dimensional numerical simulation. Energy Convers Manage 2016;117:206–17.
[44] Sobhani E, Ghaffari M, Maghrebi MJ. Numerical investigation of dimple effects on darrieus vertical axis wind turbine. Energy 2017;133:231–41.
[45] Wang Y, Sun X, Dong X, Zhu B, Huang D, Zheng Z. Numerical investigation on aerodynamic performance of a novel vertical axis wind turbine with adaptive blades. Energy Convers Manage 2016;108:275–86.
[46] Wang Z, Zhuang M. Leading-edge serrations for performance improvement on a vertical-axis wind turbine at low tip-speed-ratios. Appl Energy 2017. http://dx.doi.org/10.1016/j.apenergy.2017.09.034.
[47] Simão Ferreira C, van Zuijlen A, Bijl H, van Bussel G, van Kuik G. Simulating dynamic stall in a two-dimensional vertical-axis wind turbine: verification and validation with particle image velocimetry data. Wind Energy 2010;13(1):1–17.
[48] Trivellato F, Raciti Castelli M. On the Courant–Friedrichs–Lewy criterion of rotating grids in 2D vertical-axis wind turbine analysis. Renew Energy 2014;62:53–62.
[49] Elkhoury M, Kiwata T, Aoun E. Experimental and numerical investigation of a three-dimensional vertical-axis wind turbine with variable-pitch. J Wind Eng Ind Aerodyn 2015;139:111–23.
[50] Balduzzi F, Bianchini A, Maleci R, Ferrara G, Ferrari L. Critical issues in the CFD simulation of Darrieus wind turbines. Renew Energy 2016;85:419–35.
[51] Shahizare B, Bin Nazri, Nik Ghazali N, Chong W, Tabatabaeikia S, Izadyar N. Investigation of the optimal omni-direction-guide-vane design for vertical axis wind turbines based on unsteady flow CFD simulation. Energies 2016;9(3):146.
[52] Biswas A, Gupta R, Sharma KK. Experimental investigation of overlap and blockage effects on three-bucket Savonius rotors. Wind Eng 2007;31(5):363–8.
[53] Ross I, Altman A. Wind tunnel blockage corrections: review and application to Savonius vertical-axis wind turbines. J Wind Eng Ind Aerodyn 2011;99(5):523–38.
[54] Beri H, Yao Y. Effect of camber airfoil on self starting of vertical axis wind turbine. J Environ Sci Technol 2011;4(3):302–12.
[55] Rossetti A, Pavesi G. Comparison of different numerical approaches to the study of the H-darrieus turbines start-up. Renew Energy 2013;50:7–19.
[56] Mohamed MH. Performance investigation of H-rotor Darrieus turbine with new airfoil shapes. Energy 2012;47(1):522–30.
[57] Ikoma T, Masuda K, Fujio S, Nakada H, Maeda H. Characteristics of hydrodynamic forces and torque on darrieus type water turbines for current power generation systems with CFD computations. In: OCEANS 2008 – MTS/IEEE Kobe Techno-Ocean, Kobe, Japan; April 8–11 2008.
[58] Simão Ferreira C. The near wake of the VAWT: 2D and 3D views of the VAWT aerodynamics PhD TU Delft; 2009.
[59] Menter FR, Langtry RB, Likki SR, Suzen YB, Huang PG, Völker S. A correlation-based transition model using local variables—part I: model formulation. J Turbomach 2006;128(3):413–22.
[60] Menter FR. Two-equation eddy-viscosity turbulence models for engineering applications. AIAA J 1994;32(8):1598–605.
[61] Menter FR, Kuntz M, Langtry R. Ten years of industrial experience with the SST turbulence model. In: Turbulence, heat and mass transfer, vol. 4, ed; 2003.
[62] Menter FR, Langtry R, Völker S. Transition modelling for general purpose CFD codes. Flow Turbul Combust 2006;77(1–4):277–303.
[63] Langtry RB, Menter FR, Likki SR, Suzen YB, Huang PG, Völker S. A correlation-based transition model using local variables—part II: test cases and industrial applications. J Turbomach 2006;128(3):423–34.
[64] Suzen YB, Huang PG. Modeling of flow transition using an intermittency transport equation. NASA/CR-1999-209313; 1999.
[65] Suzen YB, Huang PG, Hultgren LS, Ashpis DE. Predictions of separated and transitional boundary layers under low-pressure turbine airfoil conditions using an intermittency transport equation. J Turbomach 2003;125(3):455.
[66] Walters DK, Leylek JH. A new model for boundary layer transition using a single-point RANS approach. J Turbomach 2004;126(1):193.
[67] Cutrone L, De Palma P, Pascazio G, Napolitano M. Predicting transition in two- and three-dimensional separated flows. Int J Heat Fluid Flow 2008;29(2):504–26.
[68] Genç MS, Kaynak Ü, Lock GD. Flow over an aerofoil without and with leading edge slat at a transitional Reynolds number. In: Proc IMechE, Part G – journal of aerospace engineering; 2009. p. 217–31.
[69] Genç MS. Numerical simulation of flow over a thin aerofoil at a high reynolds number using a transition model. Proc Inst Mech Eng Part C: J Mech Eng Sci 2010:2155–22164.
[70] Genç MS, Kaynak Ü, Yapici H. Performance of transition model for predicting low

aerofoil flows without/with single and simultaneous blowing and suction. Eur J Mech B Fluids 2011;30(2):218–35.
[71] Genç MS, Karasu I, Açikel HH. Low Reynolds number flows and transition. In: Genç MS, editor. Low Reynolds number aerodynamics and transition. InTech-Open Access Publishing; 2012.
[72] Genç MS, Karasu İ, Hakan Açıkel H. An experimental study on aerodynamics of NACA2415 aerofoil at low Re numbers. Exp Thermal Fluid Sci 2012;39:252–64.
[73] Karasu I, Genç MS, Açikel HH. Numerical study on low Reynolds number flows over an aerofoil. J Appl Mech Eng 2013;02(05).
[74] Menter FR. Zonal two equation k·omega turbulence models for aerodynamic flows. 24th fluid dynamics conference, Orlando, Florida. 1993.
[75] ANSYS. ANSYS® Fluent theory guide, release 16.1, ANSYS Inc; 2015.
[76] Roache PJ. Quantification of uncertainty in computational fluid dynamics. Annu Rev Fluid Mech 1997;29:123–60.
[77] Castelli MR, Englaro A, Benini E. The Darrieus wind turbine: proposal for a new performance prediction model based on CFD. Energy 2011;36(8):4919–34.
[78] Castelli MR, Ardizzon G, Battisti L, Benini E, Pavesi G. Modeling strategy and numerical validation for a Darrieus vertical axis micro-wind turbine. In: ASME 2010 international mechanical engineering congress & exposition. British Columbia, Canada: Vancouver; 2010.
[79] Lardeau S, Leschziner MA. Unsteady RANS modelling of wake–blade interaction: computational requirements and limitations. Comput Fluids 2005;34(1):3–21.
[80] Rockwell D. Vortex-body interactions. Annu Rev Fluid Mech 1998;30:199–229.
[81] Bachant P, Wosnik M. Effects of Reynolds number on the energy conversion and near-wake dynamics of a high solidity vertical-axis cross-flow turbine. Energies 2016;9(73).
[82] Vermeer L, Sørensen JN, Crespo A. Wind turbine wake aerodynamics. Prog Aerosp Sci 2003;39:467–510.